



Supplement of

Nutrient utilisation and weathering inputs in the Peruvian upwelling region since the Little Ice Age

C. Ehlert et al.

Correspondence to: C. Ehlert (cehlert@mpi-bremen.de)

1 **Supplementary material**

2

3 **Nutrient Utilisation and Weathering Inputs in the**
4 **Peruvian Upwelling Region Since the Little Ice Age**

5

6 **C. Ehler, P. Grasse, D. Gutiérrez, R. Salvatteci and M. Frank**

7

8 **1 Age model for core M771-470**

9 Core M771-470 was taken at 11° S, 77°56.6' W in 145 m water depth during cruise
10 M77/1 with the German R/V Meteor in 2008 (Fig. 1). The age model was obtained by
11 measuring excess ^{210}Pb activities and modeling the resulting profiles as described by
12 Meysman et al. (2005) (Fig. S1, Table S1). Porosity data for core M771-470 were
13 determined from water loss after freeze-drying. The fit to the porosity data was
14 obtained by applying Φ_0 (porosity at the sediment water interface) = 0.95, Φ_f (porosity
15 at infinite depth after steady state compaction) = 0.85, p (attenuation constant) = 0.02
16 cm^{-1} . Excess ^{210}Pb was modelled based on a fit to the data obtained with $D_B(0)$
17 (bioturbation coefficient at the sediment water interface) = 30 $\text{cm}^2 \text{ yr}^{-1}$, x_s (sediment
18 depth where $D_B(x)$ is approaching a value of zero) = 7 cm, A_I (^{210}Pb activity of the
19 particles raining to the seafloor) = 3.4 Bq g^{-1} , w_f (burial velocity) = 48 cm kyr^{-1} . These
20 results indicate bioturbation in the uppermost 10 cm. The average sedimentation rate
21 of core M771-470 between 10 and 25cm profile depth of 0.92 mm/yr is essentially
22 identical to the one obtained from the nearby core SO147-106KL for the time period
23 1400-1900 AD of 0.9 mm/yr (Rein et al., 2004).

24 The porosity data show a pronounced decrease between 24 cm and 32 cm profile
25 depth (Fig. S.1a and Fig. 2, Table S.1), which is considered to reflect a
26 sedimentological feature that marks the transition of the LIA towards modern
27 conditions (= transition period). This shift can be found in several cores from the
28 region and has been dated to start ~1820 AD, with an uncertainty of 10-15 years
29 (Gutiérrez et al., 2009; Salvatteci et al., in review). The highest values of bSi that can
30 be found in ~25 cm profile depth in core M771-470 are recorded in several cores off

1 Peru and Chile just after the LIA during the transition period (Gutiérrez et al., 2009;
2 Díaz-Ochoa et al., 2011; Salvatteci et al. in review), suggesting a regional event.
3 Using average sedimentation rates from the nearby core B0405-13 (12°S, 184 m
4 water depth) of ~1.8 mm/yr for the modern sediments from the time period 1870-1952
5 AD, ~1.5 mm/yr for the transition period between 1818-1870 AD and lower
6 sedimentation rates of 0.6 mm/yr during the LIA from ca. 1300-1818 AD (Gutiérrez
7 et al., 2009) would indicate, that the core depth between 26 cm and 32 cm
8 corresponds to the transition period, shallower depths reflect modern sediments and
9 deeper depths reflect sediments from the LIA. This was adopted for the discussion in
10 the manuscript.

11

12 **2 Leachate neodymium isotope composition**

13 **2.1 Methods**

14 To obtain the radiogenic isotope composition of past bottom seawater at the sites of
15 the sediment cores from the early diagenetic Fe-Mn coatings of the sediment particles,
16 previously published methods were applied (Gutjahr et al., 2007; Stumpf et al., 2010).
17 First, the carbonate fraction was removed from the freeze-dried and homogenized
18 sediment samples using a 15%-acetic acid/1 M Na-acetate buffer solution.
19 Afterwards, the authigenic Fe-Mn oxyhydroxide fraction was leached and separated
20 from the sediment with a 0.05 M hydroxylamine hydrochloride/15%-acetic acid
21 solution buffered with NaOH to pH 3.8. For purification of the leachate fraction and
22 analyses of Nd and Sr isotope composition please refer to the main text.

23

24 **2.2 Changes in Subsurface Water Masses**

25 The ε_{Nd} coating record of core M771-470 only shows a small variability ranging from -
26 1.2 to -2.3 with a mean value of -1.7 ± 0.7 ($2\sigma_{(\text{sd})}$) and no significant trends are
27 observable (Fig. S2, Table S2). For core B0405-6 no ε_{Nd} coating signature could be
28 determined because the available amount of left over sediment material was not
29 sufficient.

30 Knowledge about changes in the origin of the subsurface waters would help to better
31 constrain some of the changes in utilisation discussed, i.e. concerning the source

1 regions (northern or southern) of the water masses and therefore which pre-formed
2 (utilisation) signal should be assumed. Early diagenetic Fe-Mn coatings in marine
3 sediments have been shown to archive the dissolved ε_{Nd} signature of (bottom) water
4 masses, which had been acquired in the source regions of water masses via
5 weathering of continental rocks with distinct isotopic signatures and supply to the
6 ocean via rivers, eolian input or through shelf exchange processes (Frank, 2002;
7 Lacan and Jeandel, 2005). The Eastern Equatorial Pacific is influenced by two main
8 water mass sources. The Central Pacific is characterised by more radiogenic
9 signatures around -2 and waters of this origin are supplied to the EEP via the
10 EUC/PCUC (Fig. 1) (Lacan and Jeandel, 2001; Grasse et al., 2012). In contrast, the
11 water masses of Southern Ocean origin are characterised by less radiogenic signatures
12 around -8 (Piepgras and Jacobsen, 1988; Grasse et al., 2012). Core M771-470 is
13 located in 145 m water depth, which is in the present day core depth of the PCUC
14 (Fig. 1) (Brink et al., 1983). The ε_{Nd} coating signature in core M771-470 ranges between
15 -1.2 and -2.3, which suggests that the signature has not deviated significantly from the
16 composition of the present-day PCUC (Grasse et al., 2012; Ehlert et al., 2013). As
17 described above, the PCUC is the predominant bottom current at the location of the
18 core under strong upwelling conditions. When upwelling was weak the surface
19 currents could expand both latitudinally and vertically within the water column and
20 may also have impacted the bottom water signatures (Montes et al., 2011). However,
21 as described by Ehlert et al. (2013), the variability of the ε_{Nd} coating signature on the
22 Peruvian shelf has not necessarily only been related to the prevalent current regime
23 and water mass mixing but exchange between bottom waters and the underlying
24 sediments and the pore waters plays an important role, in particular under oxygen-
25 depleted conditions in the sediments and bottom waters (Haley et al., 2004; Lacan and
26 Jeandel, 2005), which prevents a reliable assessment of past water mass mixing based
27 on the Nd isotope composition of the coatings. This is the reason why the data for the
28 one core are not included in the discussion of the main text and only provided here for
29 completeness.

30

31 **Supplementary references**

32 Brink, K. H., Halpern, D., Huyer, A., and Smith, R. L.: The Physical Environment of
33 the Peruvian Upwelling System, *Progress in Oceanography*, 12, 285–305, 1983.

1 Díaz-Ochoa, J. A., Pantoja, S., De Lange, G. J., Lange, C. B., Sánchez, G. E., Acuña,
2 V. R., Muñoz, P., and Vargas, G.: Oxygenation variability in Mejillones Bay, off
3 northern Chile, during the last two centuries, *Biogeosciences*, 8(1), 137–146, 2011.
4 doi:10.5194/bg-8-137-2011

5 Ehlert, C., Grasse, P., and Frank, M.: Changes in silicate utilisation and upwelling
6 intensity off Peru since the Last Glacial Maximum - insights from silicon and
7 neodymium isotopes, *Quaternary Science Reviews*, 72, 18–35, 2013.
8 doi:10.1016/j.quascirev.2013.04.013

9 Frank, M.: Radiogenic isotopes: tracers of past ocean circulation and erosional input,
10 *Reviews of Geophysics*, 40(1), 2002. doi:10.1029/2000RG000094

11 Grasse, P., Stichel, T., Stumpf, R., Stramma, L., and Frank, M.: The distribution of
12 neodymium isotopes and concentrations in the Eastern Equatorial Pacific: Water mass
13 advection versus particle exchange, *Earth and Planetary Science Letters*, 353-354,
14 198–207, 2012. doi:10.1016/j.epsl.2012.07.044

15 Gutiérrez, D., Sifeddine, A., Field, D. B., Ortlieb, L., Vargas, G., Chavez, F. P.,
16 Velazco, F., Ferreira-Bartrina, V., Tapia, P. M., Salvatteci, R., Boucher, H., Morales,
17 M. C., Valdés, J., Reyss, J.-L., Campusano, A., Boussafir, M., Mandeng-Yogo, M.,
18 García, M., and Baumgartner, T.: Rapid reorganization in ocean biogeochemistry off
19 Peru towards the end of the Little Ice Age, *Biogeosciences*, 6, 835–848, 2009.

20 Gutjahr, M., Frank, M., Stirling, C. H., Klemm, V., Van de Flierdt, T., and Halliday,
21 A. N.: Reliable extraction of a deepwater trace metal isotope signal from Fe–Mn
22 oxyhydroxide coatings of marine sediments, *Chemical Geology*, 242, 351–370, 2007.
23 doi:10.1016/j.chemgeo.2007.03.021

24 Haley, B. A., Klinkhammer, G. P., and McManus, J.: Rare earth elements in pore
25 waters of marine sediments, *Geochimica et Cosmochimica Acta*, 68(6), 1265–1279,
26 2004. doi:10.1016/j.gca.2003.09.012

27 Lacan, F., and Jeandel, C.: Tracing Papua New Guinea imprint on the central
28 Equatorial Pacific Ocean using neodymium isotopic compositions and Rare Earth
29 Element patterns, *Earth and Planetary Science Letters*, 186, 497–512, 2001.

1 Lacan, F., and Jeandel, C.: Neodymium isotopes as a new tool for quantifying
2 exchange fluxes at the continent – ocean interface, *Earth and Planetary Science
3 Letters*, 232, 245–257, 2005. doi:10.1016/j.epsl.2005.01.004

4 Meysman, F. J. R., Boudreau, B. P., and Middelburg, J. J.: Modeling reactive
5 transport in sediments subject to bioturbation and compaction, *Geochimica et
6 Cosmochimica Acta*, 69(14), 3601–3617, 2005. doi:10.1016/j.gca.2005.01.004

7 Montes, I., Schneider, W., Colas, F., Blanke, B., and Echevin, V.: Subsurface
8 connections in the eastern tropical Pacific during La Niña 1999 – 2001 and El Niño
9 2002 – 2003, *Journal of Geophysical Research*, 116(C12022), 2011.
10 doi:10.1029/2011JC007624

11 Piepgras, D. J., and Wasserburg, G. J.: Isotopic Composition of Neodymium in
12 Waters from the Drake Passage, *Science*, 217, 207–214, 1982.

13 Rein, B., Lückge, A., and Sirocko, F.: A major Holocene ENSO anomaly during the
14 Medieval period, *Geophysical Research Letters*, 31(L17211), 2004.
15 doi:10.1029/2004GL020161

16 Salvatteci, R., Field, D. B., Sifeddine, A., Ortlieb, L., Ferreira-Bartrina, V.,
17 Baumgartner, T., Caquineau, S., Velazco, F., Reyss, J.-L., Sanchez-Cabeza, J. A., and
18 Gutiérrez, D.: Cross-stratigraphies from a seismically active mud lens off Peru
19 indicate horizontal extensions of laminae, missing sequences, and a need for multiple
20 cores for high resolution records, *Marine Geology* (in review).

21 Stumpf, R., Frank, M., Schönfeld, J., and Haley, B. A.: Late Quaternary variability of
22 Mediterranean Outflow Water from radiogenic Nd and Pb isotopes, *Quaternary
23 Science Reviews*, 49, 1–11, 2010. doi:10.1016/j.quascirev.2010.06.021

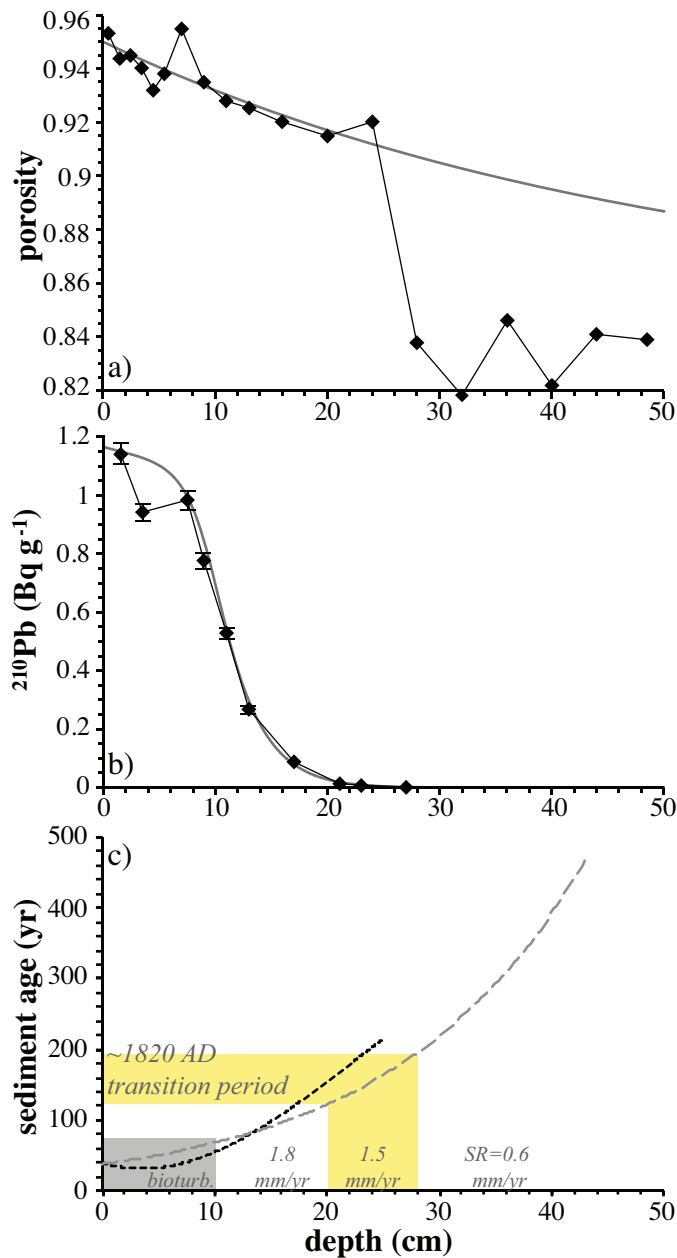
24

1 Table S1. Core M771-470 a) excess ^{210}Pb measurements and porosity data, b) age
 2 model based on sedimentation rates from Gutiérrez et al. (2009), and $^{143}\text{Nd}/^{144}\text{Nd}$, ε_{Nd}
 3 and $^{87}\text{Sr}/^{86}\text{Sr}$ of authigenic Fe-Mn coatings. $2\sigma_{(\text{sd})}$ represents the external
 4 reproducibilities of repeated standard measurements.

| a) ^{210}Pb -dating and porosity | | | | b) age model | | | | | | | |
|---|---------------------------|---------------|----------|--------------|------------|---------|-----------------------------------|---------------------------|-------------------------|---------------------------------|-------------------------|
| depth (cm) | ^{210}Pb (Bq/kg) | error (Bq/kg) | porosity | depth (cm) | Sed. rate* | year AD | $^{143}\text{Nd}/^{144}\text{Nd}$ | ε_{Nd} | $2\sigma_{(\text{sd})}$ | $^{87}\text{Sr}/^{86}\text{Sr}$ | $2\sigma_{(\text{sd})}$ |
| 0 - 1 | - | - | 0.953 | 1.5 | | 1976 | 0.512539 | -1.9 | 0.3 | 0.709030 | 2.6E-05 |
| 1 - 2 | 1.14E+03 | 7.34E+01 | 0.944 | 3.5 | | 1965 | 0.512551 | -1.7 | 0.3 | 0.708971 | 2.6E-05 |
| 2 - 3 | - | - | 0.945 | 5.5 | | 1954 | 0.512546 | -1.8 | 0.3 | 0.709080 | 2.6E-05 |
| 3 - 4 | 9.42E+02 | 5.97E+01 | 0.940 | 9 | 1.8 mm/yr | 1934 | 0.512556 | -1.6 | 0.3 | 0.709099 | 2.6E-05 |
| 4 - 5 | - | - | 0.932 | 11 | | 1923 | 0.512526 | -2.2 | 0.3 | 0.709121 | 2.6E-05 |
| 5 - 6 | - | - | 0.938 | 15 | | 1901 | 0.512521 | -2.3 | 0.3 | 0.709112 | 2.6E-05 |
| 6 - 8 | 9.84E+02 | 6.36E+01 | 0.955 | 19 | | 1879 | 0.512559 | -1.5 | 0.3 | 0.709094 | 2.6E-05 |
| 8 - 10 | 7.75E+02 | 5.35E+01 | 0.935 | 20 | | 1873 | 0.512571 | -1.3 | 0.3 | 0.708748 | 8.0E-06 |
| 10 - 12 | 5.28E+02 | 3.74E+01 | 0.928 | 23 | | 1853 | 0.512547 | -1.8 | 0.3 | 0.709153 | 2.6E-05 |
| 12 - 14 | 2.66E+02 | 2.57E+01 | 0.925 | 25 | 1.5 mm/yr | 1840 | 0.512539 | -1.9 | 0.3 | 0.709132 | 2.6E-05 |
| 16 - 18 | 8.68E+01 | 1.86E+01 | 0.920 | 26 | | 1833 | - | - | - | 0.708973 | 8.0E-06 |
| 20 - 22 | 1.27E+02 | 1.97E+01 | 0.915 | 27 | | 1827 | 0.512542 | -1.9 | 0.3 | 0.709130 | 2.6E-05 |
| 22 - 24 | 9.49E+01 | 1.87E+01 | 0.920 | 29 | | 1803 | 0.512538 | -2 | 0.3 | 0.709136 | 2.6E-05 |
| 26 - 28 | <2.28E+01 | - | 0.838 | 32 | | 1753 | 0.512523 | -2.3 | 0.3 | 0.709140 | 2.6E-05 |
| 28 - 30 | <2.08E+01 | - | - | 32 (dupl.) | | 1753 | 0.512564 | -1.4 | 0.3 | 0.708935 | 5.0E-06 |
| 30 - 34 | <1.89E+01 | - | 0.818 | 36 | 0.6 mm/yr | 1687 | 0.512574 | -1.2 | 0.3 | 0.708727 | 8.0E-06 |
| 34 - 38 | <2.22E+01 | - | 0.846 | 40 | | 1620 | 0.512565 | -1.4 | 0.3 | 0.708928 | 8.0E-06 |
| 40 | - | - | 0.822 | 44 | | 1553 | 0.512572 | -1.3 | 0.3 | 0.708745 | 5.0E-06 |
| 44 | - | - | 0.841 | 48.5 | | 1478 | 0.512564 | -1.4 | 0.3 | 0.708847 | 5.0E-06 |
| 48.5 | - | - | 0.839 | | | | | | | | |

5 *average sedimentation rates were determined on nearby core B0405-13.

6



1

2 Figure S1. Age model for core M771-470 (data: black diamonds, best fit: grey line).
3 a) porosity versus depth (cm), b) excess ^{210}Pb activity (Bq g^{-1}), and c) resulting
4 age/depth relationship (black curve = ^{210}Pb modeling, grey curve = using average
5 sedimentation rates of core B0405-13 (Gutiérrez et al., 2009). The grey shading
6 indicates the bioturbated zone, the yellow shading highlights the transition zone from
7 the LIA to modern sediments.

8

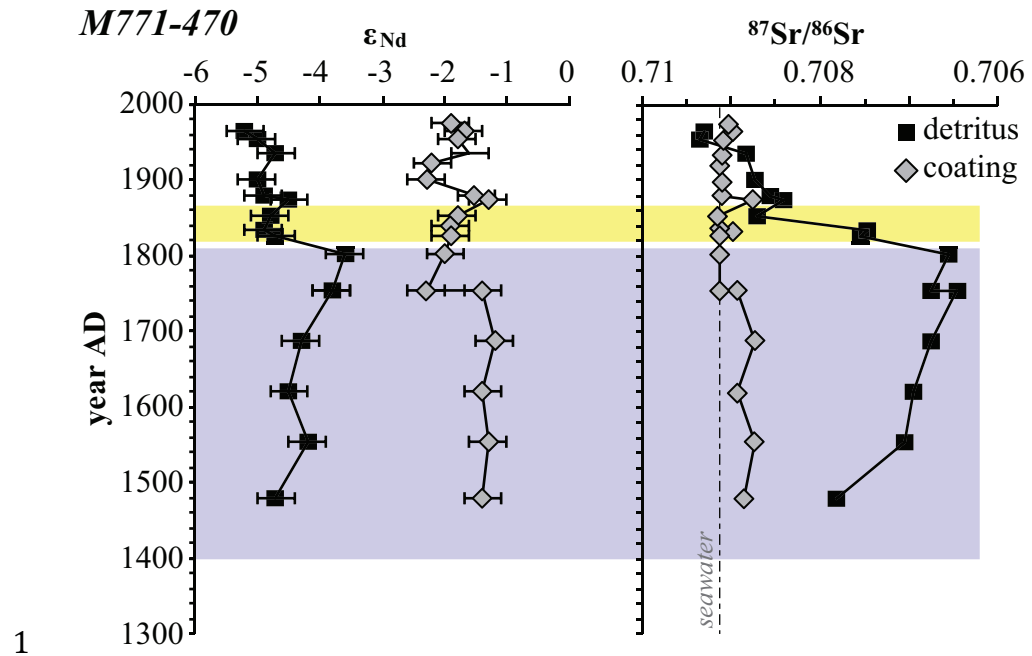


Figure S2. Downcore records for core M771-470 for ϵ_{Nd} and $^{87}\text{Sr}/^{86}\text{Sr}$ for authigenic Fe-Mn coatings (grey diamonds) and detrital material (black squares). Error bars represent $2\sigma_{(\text{sd})}$ external reproducibilities of repeated standard measurements. The grey dashed line indicates the present day dissolved seawater $^{87}\text{Sr}/^{86}\text{Sr}$ of 0.70916. The blue shading indicates the LIA and the yellow shading represents the time span of the transition period.